



**HAL**  
open science

## Subcellular Chemical Imaging: New Avenues in Cell Biology.

Johan Decelle, Giulia Veronesi, Benoit Gallet, Hryhoriy Stryhanyuk, Pietro Benettoni, Matthias Schmidt, Rémi Tucoulou, Melissa Passarelli, Sylvain Bohic, Peta Clode, et al.

► **To cite this version:**

Johan Decelle, Giulia Veronesi, Benoit Gallet, Hryhoriy Stryhanyuk, Pietro Benettoni, et al.. Subcellular Chemical Imaging: New Avenues in Cell Biology.. Trends in Cell Biology, 2020, 30 (3), pp.173-188. 10.1016/j.tcb.2019.12.007 . hal-02492213

**HAL Id: hal-02492213**

**<https://hal.science/hal-02492213>**

Submitted on 23 Nov 2020

**HAL** is a multi-disciplinary open access archive for the deposit and dissemination of scientific research documents, whether they are published or not. The documents may come from teaching and research institutions in France or abroad, or from public or private research centers.

L'archive ouverte pluridisciplinaire **HAL**, est destinée au dépôt et à la diffusion de documents scientifiques de niveau recherche, publiés ou non, émanant des établissements d'enseignement et de recherche français ou étrangers, des laboratoires publics ou privés.



Distributed under a Creative Commons Attribution - NoDerivatives 4.0 International License

# 1 Subcellular chemical imaging: new avenues in cell biology

2 Johan Decelle<sup>1\*</sup>, Giulia Veronesi<sup>2,3</sup>, Benoit Gallet<sup>4</sup>, Hryhoriy Stryhanyuk<sup>5</sup>, Pietro Benettoni<sup>5</sup>, Matthias  
3 Schmidt<sup>5</sup>, Rémi Tucoulou<sup>3</sup>, Melissa Passarelli<sup>6</sup>, Sylvain Bohic<sup>3,7</sup>, Peta Clode<sup>8,9</sup>, Niculina Musat<sup>5</sup>

## 4 **Affiliations:**

5 1- Cell and Plant Physiology Laboratory, University Grenoble Alpes, CNRS, CEA, INRA, IRIG, Grenoble, France.

6 2- Chemistry and Biology of Metals Laboratory, Université Grenoble Alpes, CNRS, CEA, IRIG, Grenoble, France.

7 3- ESRF - The European Synchrotron, Grenoble, France.

8 4- Institut de Biologie Structurale, Université Grenoble Alpes, CNRS, CEA; Grenoble, France.

9 5- Helmholtz Centre for Environmental Research – UFZ, Department of Isotope Biogeochemistry, Leipzig, Germany.

10 6- Ecole Polytechnique Fédérale de Lausanne (EPFL), Laboratory for Biological Geochemistry, Lausanne, Switzerland.

11 7- INSERM – UA7 – Synchrotron Radiation for Biomedicine, STROBE, University Grenoble Alpes, Grenoble, France.

12 8- The Centre for Microscopy Characterisation and Analysis, The University of Western Australia, Crawley, Australia.

13 9- UWA School of Biological Sciences, The University of Western Australia, Crawley, Australia.

14

15 **Keywords:** chemical imaging, correlative microscopy, electron microscopy, elemental imaging,  
16 X-ray fluorescence, SIMS

17 \*Correspondence: [johan.decelle@univ-grenoble-alpes.fr](mailto:johan.decelle@univ-grenoble-alpes.fr)

18

## 19 **Abstract**

20 To better understand the physiology and acclimation capability of a cell, one of the great challenges  
21 of the future is to access the interior of a cell and unveil its chemical landscape (composition and  
22 distribution of elements and molecules). Chemical imaging has greatly improved in sensitivity and  
23 spatial resolution to visualize and quantify nutrients, metabolites, toxic elements, and drugs in  
24 single cells at the subcellular level. This review aims at presenting the current potential of these  
25 emerging imaging technologies and guiding biologists towards a strategy for interrogating  
26 biological processes at the nanoscale. We also describe different solutions to combine multiple  
27 imaging techniques in a correlative way and provide perspectives and future directions for  
28 integrative subcellular imaging across different disciplines.

29

## 30 New avenues for the subcellular exploration of the cell

31 The advent of electron microscopy in the mid 1900s was a formidable tool for the detailed  
32 exploration of a cell's structure at nanoscale resolution. Nowadays, a key challenge in cell biology  
33 is to understand the activity and function of organelles and cellular compartments, and their role  
34 in the metabolism and physiology of a cell. *Omic*s bulk analyses (e.g. transcriptomics,  
35 metabolomics) have greatly improved our understanding on cellular mechanisms, but only provide  
36 averaged information of extracted molecules from numerous lysed cells. Hence, spatial  
37 information at the subcellular level is a missing dimension to fully interpret the phenotypic state  
38 of a cell and assess heterogeneity in a population. **Chemical imaging** techniques (see Glossary)  
39 are now able to reveal the **chemical landscape** of cells (*i.e.* the composition and distribution of  
40 elements and molecules) at the subcellular level without the need to add or genetically encode  
41 fluorescent labels. Probing the elemental and molecular composition in organelles and subcellular  
42 structures can reveal fundamental information about the function and physiology of a cell in  
43 response to different conditions. The subcellular distribution of some elements (e.g. the  
44 macronutrients N, P, S), which are essential building blocks of biomolecules (e.g. DNA, proteins,  
45 lipids), can reflect the metabolic roles and needs of organelles [1]. Trace metals (e.g. Fe, Cu, Zn)  
46 play a fundamental role in different biochemical functions of the cell, and their homeostasis and  
47 compartmentalization need to be tightly controlled to avoid cell death and severe pathologies.  
48 More particularly, metals are key players in parasitic and viral infections, cancer cells, and  
49 neurodegenerative diseases [2]. In the biomedical field, the increasing human exposure to  
50 exogenous compounds (e.g. metal-based nanoparticles, toxic elements) and use of therapeutic  
51 drugs, call for imaging techniques to visualize their fate in tissues and cells, and assess their  
52 toxicity and impact on the homeostasis of native elements [3,4]. In addition to elements, the  
53 localization of metabolites (e.g. sugars, lipids) in cells is also essential to fully understand  
54 metabolic processes. Therefore, subcellular mapping of elements and metabolites is becoming  
55 indispensable to investigate the physiology and metabolism of healthy and diseased cell types,  
56 understand cellular interactions in tissues or with beneficial cells (e.g. symbioses) and pathogens  
57 (e.g. viral or bacterial infection), and their adaptive response to abiotic stresses.

58 Recent technological progress in chemical imaging has substantially improved sensitivity and  
59 spatial resolution, allowing disentangling of cellular compartments in a single cell. However, the  
60 multiplicity of these complex imaging techniques requires guidance for non-specialists. An

61 overview of the chemical imaging techniques currently available is therefore needed to help  
62 biologists integrating the subcellular scale in their studies while being aware of their potential and  
63 limitations. Each chemical imaging platform presents experimental specifications that make them  
64 more sensitive to some elements or molecules, so different platforms need to be combined to have  
65 a comprehensive view of the chemical landscape of a cell. Moreover, since chemical imaging  
66 generally provides limited information on the cell ultrastructure, electron microscopy (EM) is often  
67 required to interpret the intracellular localization of elements and molecules. Correlation between  
68 light microscopy and EM (CLEM) is well established [5,6], but correlation between EM and  
69 chemical imaging is less developed. Bridging the data acquired with different high-resolution  
70 imaging strategies is the next challenge and will make correlative subcellular imaging a new  
71 powerful research tool towards integrative cell biology.

72 This review aims at presenting the potential and limitations of state-of-the-art chemical imaging  
73 techniques for non-specialists who seek to obtain chemical information at the subcellular level.  
74 We aim to guide biologists to the appropriate imaging technique and associated sample preparation  
75 to visualize and quantify elements or biomolecules in cells. We also summarize the new  
76 developments for correlative subcellular imaging (Figure 1, Key Figure), highlight the role of such  
77 combinatory techniques to disentangle biochemical processes of a cell and discuss future  
78 challenges and directions in the field.

79

## 80 **Potential and limitations of subcellular chemical imaging platforms and** 81 **required sample preparation**

82 Multiple chemical imaging instruments are capable of visualizing the molecular, elemental, and  
83 isotopic composition of a cell with high lateral resolution [7]. These microscopes are generally  
84 equipped with a high-energy, and focused primary beam of electrons, protons, photons, or ions  
85 that raster across the surface of the sample and obtain quantitative information in a spatially  
86 resolved manner (Box 1). The instrument and experimental setup need to be carefully chosen  
87 according to the research question and the target elements or molecules of interest. Here we focus  
88 on the key methodologies that are routinely being used to provide subcellular information. Lower  
89 resolution technologies (e.g. MALDI, LA-ICP-MS) will not be discussed in detail here (see review  
90 [8]).

91 **X-ray fluorescence microscopy** relies on the excitation of core electrons of atoms that leads to  
92 X-ray emissions, which are specific to elements in the sample (see Glossary and Box 1). The  
93 primary probe determines the technique: electrons in Energy Dispersive X-ray Spectrometry  
94 (S/TEM-EDS); protons in particle-induced X-ray emission (PIXE), synchrotron-generated  
95 photons in synchrotron X-Ray Fluorescence (S-XRF) imaging. These analytical techniques can be  
96 used to visualize and quantify the distribution of macronutrients (e.g. P, S), key trace elements  
97 (e.g. Mn, Fe, Cu, Zn, Se), toxic heavy metals (e.g. Hg, Pb), and pharmacological compounds (e.g.  
98 organometallic compounds based on Pt, Ir, Os, Ru). S/TEM-EDS can provide the highest spatial  
99 resolution (sub-nanometre in TEM) with sensitivity of  $\sim 1000$  ppm ( $1 \text{ mg}\cdot\text{g}^{-1}$ ) [9]. Compared to  
100 this, PIXE is less spatially resolved (sub-micron) but is more sensitive (ppm range) [7]. But overall,  
101 synchrotron X-ray Fluorescence (S-XRF) provides arguably the best combination of high spatial  
102 resolution capabilities (down to few 10 nm) and high sensitivity (sub-ppm) to light and heavy  
103 elements (Figure 2, Box 1) [10,11]. S-XRF has allowed mapping and quantification of metals,  
104 such as Fe, Zn, Cu in microalgal and human cells [12–14], as well as silica, drugs, organometallic  
105 molecules, and titanium oxide nanoparticles in cancer cells [2,15–19]. In combination with XRF  
106 imaging, X-ray Absorption Spectroscopy (XAS) can be performed in order to reveal the chemical  
107 speciation of a target element. XAS has disclosed the chemical transformations of indium-based  
108 nanocrystals, or of osmium-based anticancer drugs in cancer cells [20,21]. The modulations of the  
109 XAS spectra also allowed mapping the distribution of different chemical states of S (e.g. sulfate  
110 esters and inorganic sulfate) in a biological tissue, in order to understand their role in cell  
111 differentiation [22].

112 **Secondary ion mass spectrometry (SIMS)** instruments are based on the analysis of mass of  
113 elements and molecules (see Glossary). Secondary ions are sputtered away from the topmost layer  
114 of a sample by a focused primary ion beam and analyzed in a mass spectrometer (Box 1).  
115 **NanoSIMS** is a SIMS instrument particularly suitable for probing macronutrients and metals in  
116 cells at a lateral resolution down to 50 nm (Figure 2) [23–26]. For instance, P, S, Ca, Fe, Zn, Mn,  
117 and Cu have been mapped in cells [12,25,27,28]. Morphological features of the cell can be revealed  
118 by secondary electron signal (only in negative extraction mode), and from different secondary  
119 ions, such as cyanide ( $^{12}\text{C}^{14}\text{N}^-$ ) and phosphorous ( $^{31}\text{P}^-$ ) showing the overall shape and internal  
120 compartments of the cell, and the nucleus, respectively. The high mass-resolving power of  
121 nanoSIMS can also unveil the isotopic composition of a cell (i.e. being able to distinguish between

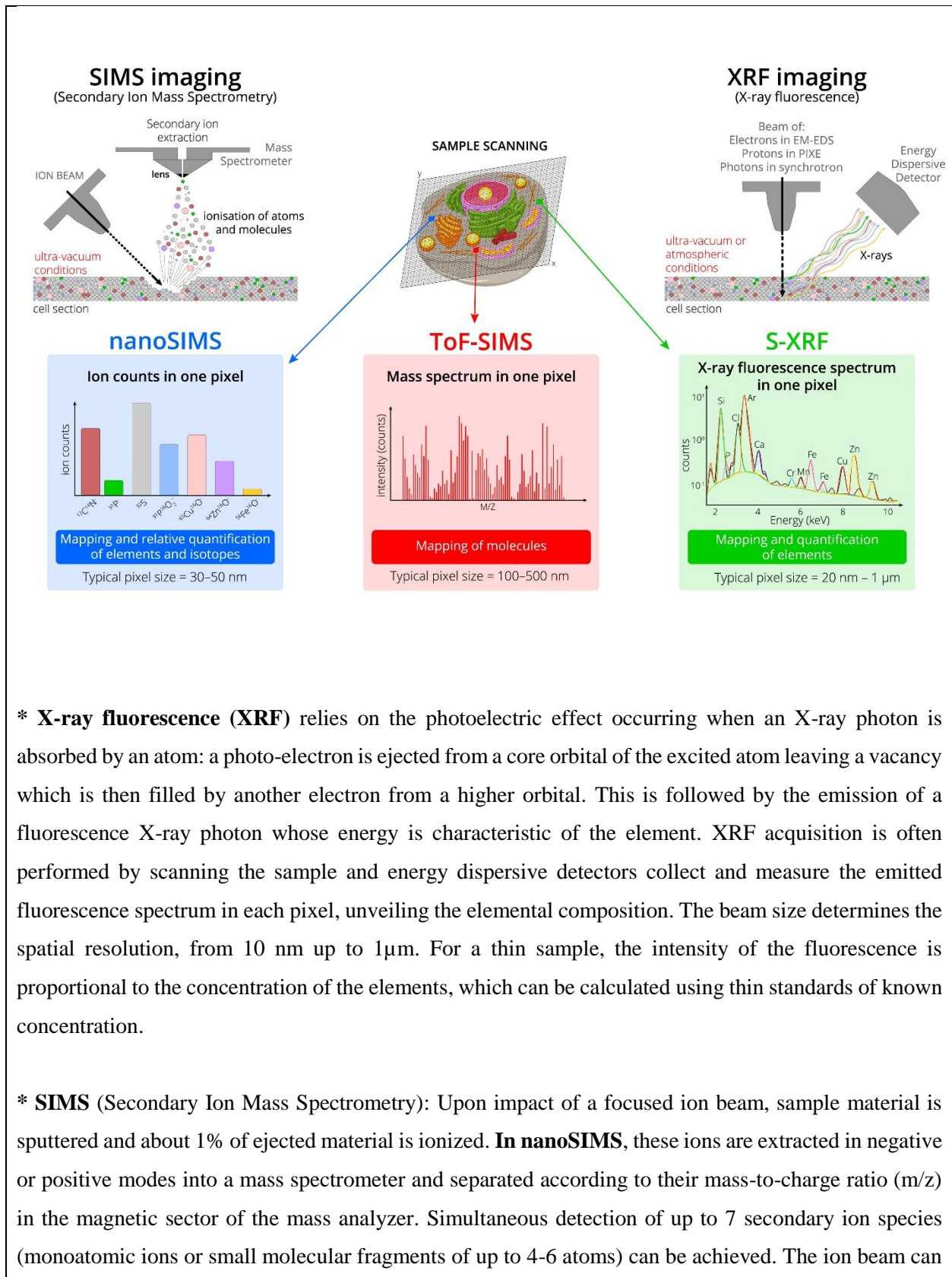
122  $^{12}\text{C}^{15}\text{N}$  and  $^{13}\text{C}^{14}\text{N}$ ), and so is highly suitable for stable isotope probing (SIP) [29,30]. SIP-  
123 nanoSIMS allows for quantitation of metabolic activities at the subcellular level (e.g. 50 - 100 nm),  
124 such as C and N assimilation [31–34]. This technique has been used to understand nutrient  
125 exchange between cells in symbiotic, pathogenic and virus-host interactions [35–40] and the  
126 localization of drug compounds in human cells [41] (Figure 2).

127 With the **ToF-SIMS** (Time-of-Flight-SIMS; see Glossary and Box 1), molecular information can  
128 be obtained since the ion probe (polyatomic or gas cluster) is less destructive than in nanoSIMS  
129 (monoatomic). The softer ionization conditions, as compared to nanoSIMS, allow for spatially  
130 resolved analysis of large molecular fragment species within the range of 1 to ~1000 Da with a  
131 typical lateral resolution of 100 nm – 5  $\mu\text{m}$ . Different analysis modes exist: spectrometry mode to  
132 get high mass resolution, imaging mode to get high lateral resolution, and delayed extraction mode  
133 to combine high mass resolution (10000 MRP) with a high lateral resolution (400 nm) [42].  
134 Delayed extraction is now widely used to image organic samples and lately was shown to achieve  
135 a 108 nm lateral resolution to visualize single particle in algal biofilms [43,44]. ToF-SIMS is a  
136 useful method for studying small molecules [45–47] and lipids in cells, especially in lipid-related  
137 diseases, such as cancer, Duchenne muscular dystrophy and atherosclerosis (Figure 2) [48,49].

138

### **Box 1. Principles of subcellular chemical imaging techniques**

**Figure\_BOX1**



scan a predefined surface area of the cell, therefore providing color-coded cartography of ion counts per pixel. Note that the charge compensation (i.e., compensating the build-up charge on non-conductive surfaces) is available only in negative extraction mode. Therefore, coating the sample surface with a conductive metal (~10 nm) is mandatory to overcome this limitation in positive extraction mode.

**In ToF-SIMS** (Time-of-Flight Secondary Ion Mass Spectrometry), the ejection and ionization of material relies on a lower ion beam fluence and less destructive cluster ion sources compared to nanoSIMS. With new cluster ion sources ( $\text{Bi}_n$ ,  $\text{Ar}_n$ ,  $\text{Au}_n$ ,  $\text{C}_{60}$ ), ToF-SIMS provides the possibility of minimizing molecular damages while maximizing molecular ion yields. Small organic molecules within range of 1 to ~1000 Da can be detected with a lateral resolution of around a micron on biological material. The pulsed operation mode of the primary ion gun and its  $45^\circ$  mounting geometry allows for charge compensation in both extraction polarities while employing the same primary ion species. Yet, the  $45^\circ$  geometry can cause shadowing and lateral displacement effect upon depth profiling or when analyzing a surface with a pronounced topography.

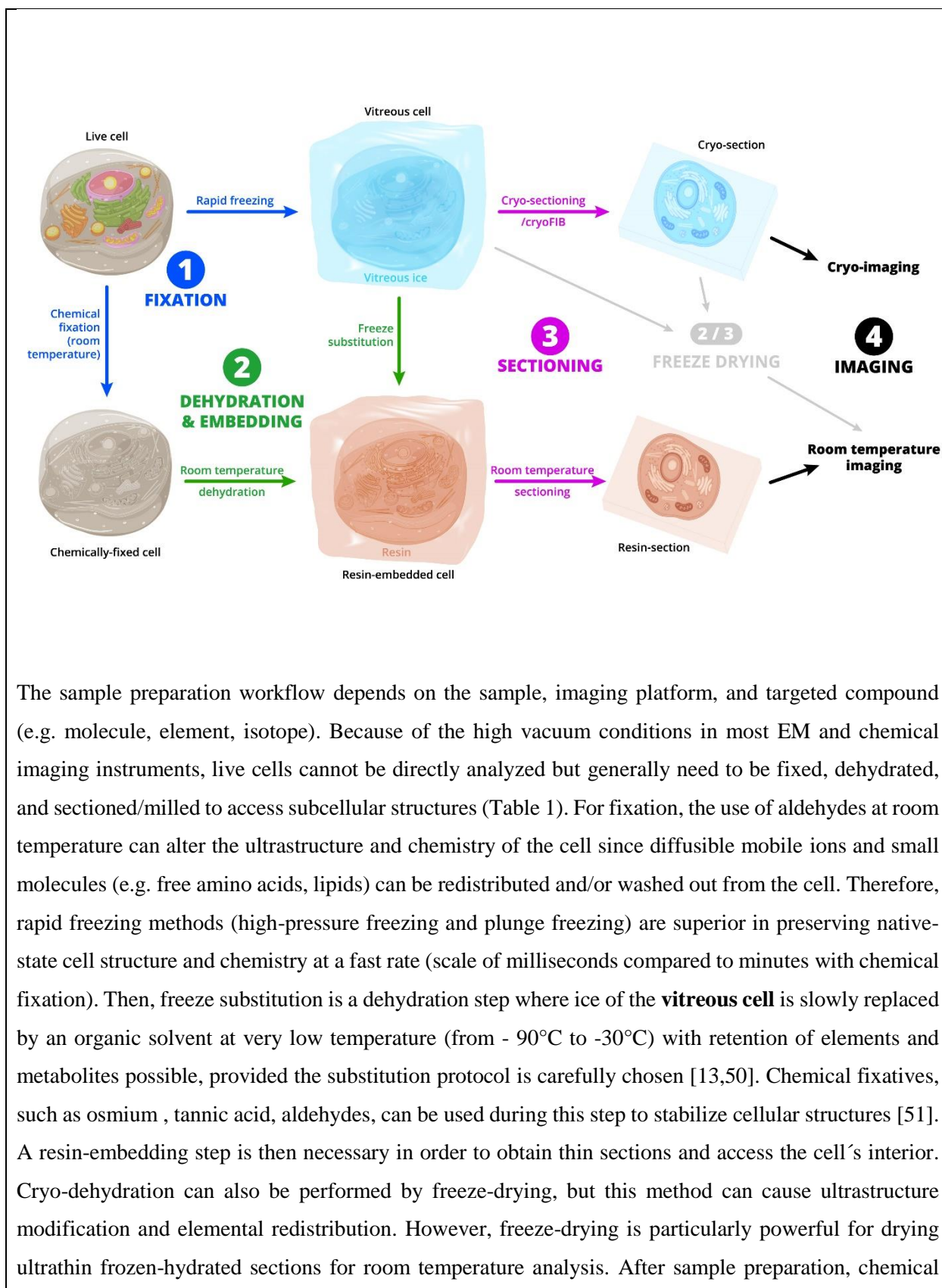
139

140 **Seeing is believing, but what we see critically depends on the sample preparation.** Sample  
141 preparation is one of the most fundamental steps – and should aim to preserve cells as close as  
142 possible to their native state - the Holy Grail in cell biology. The ideal method is the one that fixes  
143 and conserves both the ultrastructure of the cell and its native chemical composition (Box 2).  
144 However, sample preparation is highly specific to both the sample and instrument(s) being used,  
145 and compromises have to be made at each experiment (Table 1).

146

## **Box 2. Sample preparation for subcellular imaging**

**Figure Box 2**



The sample preparation workflow depends on the sample, imaging platform, and targeted compound (e.g. molecule, element, isotope). Because of the high vacuum conditions in most EM and chemical imaging instruments, live cells cannot be directly analyzed but generally need to be fixed, dehydrated, and sectioned/milled to access subcellular structures (Table 1). For fixation, the use of aldehydes at room temperature can alter the ultrastructure and chemistry of the cell since diffusible mobile ions and small molecules (e.g. free amino acids, lipids) can be redistributed and/or washed out from the cell. Therefore, rapid freezing methods (high-pressure freezing and plunge freezing) are superior in preserving native-state cell structure and chemistry at a fast rate (scale of milliseconds compared to minutes with chemical fixation). Then, freeze substitution is a dehydration step where ice of the **vitreous cell** is slowly replaced by an organic solvent at very low temperature (from -90°C to -30°C) with retention of elements and metabolites possible, provided the substitution protocol is carefully chosen [13,50]. Chemical fixatives, such as osmium, tannic acid, aldehydes, can be used during this step to stabilize cellular structures [51]. A resin-embedding step is then necessary in order to obtain thin sections and access the cell's interior. Cryo-dehydration can also be performed by freeze-drying, but this method can cause ultrastructure modification and elemental redistribution. However, freeze-drying is particularly powerful for drying ultrathin frozen-hydrated sections for room temperature analysis. After sample preparation, chemical

preservation of the cell can be assessed by visualizing the most diffusible elements ( $K^+$ ,  $Na^+$ ,  $Ca^{2+}$ ,  $Cl^-$ ) that move rapidly across membranes and within the cytoplasm, thus representing a relevant rule-of-thumb criterion for chemical preservation [52]. Overall, it remains difficult to be certain that the chemical environment within a cell is a true representation of normal physiology, and each step of the preparation can be debatable. We recommend more methodological development and comparisons in the future to optimize sample preparation and assess putative artefacts. This is a challenge since access to cutting-edge microscopes is generally difficult for that methodological purpose. Compared to freeze-substituted and resin-embedded cells, analyzing frozen-hydrated cells (or **vitreous cells**) is obviously superior for chemical preservation (Table 1). However, this leads to many challenges that need to be tackled in the future (further discussed in this review): i) cryo-sectioning, ii) the need for a cryo-transfer system and a cryo-stage in the imaging platform, iii) difficulty to undertake correlative studies across different platforms; iv) inherent lack of contrast for sample visualization.

147  
148  
149

Sample preparation steps	Strategy	Pros	Cons
Fixation of cell	Chemical fixation	Easy to use in the field or for pathogens (human parasites)	Ultrastructure and chemical composition can be greatly modified
	Cryo-fixation under high pressure	Excellent preservation of the ultrastructure and chemistry of the cell	Thickness of the sample must be less than 200 $\mu m$ , requires bulky laboratory-based equipment
	Cryo-fixation with plunge freezing in a liquid cryogen	Can be done in the field or the laboratory	Maximum sample thickness to maintain vitreous ice formation is $\sim 5 \mu m$ , some ice crystal formation in thicker samples
Dehydration	Chemical dehydration at room temperature	Can be done in the field or the laboratory	Structural and chemical preservation are not guaranteed
	Freeze-drying	No use of chemicals or solvents, ideal for drying ultrathin frozen hydrated sections for room temperature analysis	Likelihood of movement of target ions (particularly diffusible elements) or metabolites, especially in highly vacuolated tissues
	Freeze-substitution	Dehydration at very low temperature allows for good structural and chemical preservation	Use of solvents can extract materials of interest; long process (days – weeks)
Use of chemical fixative during the freeze substitution	Osmium	Membranes are fixed, and osmium provides contrast for EM investigation and structural information in XRF	Highly toxic, Interfere with some molecules and elements for XRF and ToF-SIMS analysis.
	Aldehydes	Proteins are fixed, maintaining structural preservation	Toxic, no contrast for EM investigation, cannot be prepared as anhydrous (therefore loss of any water-soluble material).

	Acrolein	Cross links at low temperatures making it highly suited for use with freeze substitution, can be anhydrous	Hazardous material
Resin Embedding	Plastic-Epoxy resin	Good structural preservation and contrast	Often contain Cl; require solvents for good infiltration
	Methacrylate resins	Preservation of antigenicity; low viscosity ideal for difficult-to-embed samples	Poor stability under an ion beam; usually require O-free environment to cure
Sectioning	Wet sectioning	Easy to collect the sections	Highly diffusible molecules can be washed out
	Dry sectioning	Avoidance of water/liquids allowing retention of water soluble ions and molecules	Difficult to cut sections thinner than 500 nm; difficult to obtain flat / uncompressed sections for analysis
Cryo-analysis	Frozen hydrated cells	The best structural and chemical preservation close to the native state, whole cells or cross sections of cells can be analyzed	Lack of contrast and structural information; correlative approaches across platforms currently difficult; cryo-sectioning (microtomy or cryo-FIB) highly specialized

150 **Table 1. Detailed procedures of the sample preparation for EM and chemical imaging, and**  
151 **considerations (Pros and cons) for each step.**  
152

### 153 Correlated subcellular imaging towards integrative cell biology

154 **Correlation between morphology and chemical imaging.** Since chemical imaging provides  
155 little morphological information, combination with light/electron microscopy is required in order  
156 to unambiguously elucidate the localization of elements and molecules within a cell. Yet, the  
157 challenge is the trade-off between ultrastructure and chemistry preservation of the cell during the  
158 sample preparation, and the ability to transfer and analyze the same cells on different imaging  
159 platforms. Some imaging techniques, such as SIMS, are destructive, meaning that morphological  
160 imaging must generally take place before. Here we propose different strategies that can be adopted  
161 to analyze the same cellular region of interest with **multimodal imaging** (Figure 1).

162 Organelles can be labeled and observed with fluorescence microscopy before the entire cell is  
163 subjected to chemical imaging. For instance, the accumulation of Mn in the Golgi apparatus of  
164 dopaminergic cells was revealed using green fluorescent proteins targeting the organelle followed  
165 by S-XRF imaging in cryogenic conditions [53–55]. More recently, correlation between super-  
166 resolution stimulated emission depletion microscopy of proteins and S-XRF imaging of trace  
167 metals were performed with 40 nm spatial resolution on neurons [56].

168 To obtain high-resolution cellular context, it is also possible to analyze cell sections in S/TEM  
169 followed by S-XRF, providing an unambiguous spatial origin of elements in subcellular

170 compartments (Figures 3 and 4) [57]. Osmium tetroxide ( $\text{OsO}_4$ ) can be used to fix and stain cellular  
171 compartments (Table 1), providing morphological contrast not only in EM, but also in S-XRF,  
172 where Os fluorescence reveals the ultrastructure of the cell (Figures 2 and 3; [12]. The drawback  
173 is that the XRF emission lines of Os interfere with those of phosphorous and some trace metals  
174 (e.g. Cu and Zn), increasing their detection limit. In order to obtain structural and  
175 elemental/isotopic information from a single cellular region, it is possible to perform TEM  
176 followed by NanoSIMS (Figure 3). Usually it would require the use of a specific TEM grid with  
177 coordinates or fiducial markers to find the same regions of interest in both instruments (Figures 3  
178 and 4) [35,37,58,59]. With the recent advent of sensitive backscatter detectors in the modern SEM  
179 it is also possible to acquire structural information from sections using SEM before nanoSIMS and  
180 S-XRF analyses, on the same sample or on consecutive sections [12,41,60].

181

182 **Correlation between fluorescence and nanoSIMS using element labeling.** The coupling  
183 between fluorescence microscopy and nanoSIMS can be a powerful approach to unveil the  
184 functional identity of a cell and organelles. This relies on targeted probing of DNA, RNA and  
185 proteins by coupling fluorescent dyes to elements usually absent from cell's natural composition,  
186 such as halogens (fluorine, bromine), gold, and boron. A specific exogenous element (detectable  
187 by nanoSIMS) can be associated/linked to fluorescent dyes, antibodies, or nanobodies, allowing  
188 correlative microscopy between fluorescence *in situ* hybridization (FISH), immunocytochemistry  
189 or click chemistry approaches with nanoSIMS [23,61,62]. For example, the nucleotide analogue,  
190 bromo-deoxyurine (BrdU), which is incorporated into replicating DNA during cell division, can  
191 be detected by fluorescence immunohistochemistry but also as bromine ions (e.g.,  $^{79}\text{Br}$ ,  $^{81}\text{Br}$ ) by  
192 nanoSIMS in the same cells [63]. Fluorine ( $^{19}\text{F}$ ) labelling of proteins using  $^{19}\text{F}$ -azide probe [64] or  
193 by conjugation to nanobodies (e.g. GFP-like proteins and antibodies) can enable correlated  
194 fluorescence and nanoSIMS imaging [65] (Figure 2). Similarly,  $^{197}\text{Au}$  can be conjugated to an  
195 antibody to recognize cellular actin and synaptophysin proteins by coupled immunofluorescence  
196 and nanoSIMS [66], while antibodies tagged with isotopically-pure elemental metal reporters (i.e.  
197 lanthanides) have been utilized to image protein expression in human breast tumor tissue sections  
198 [67]. Recently, boron linked to proteins or to nanobodies binding to proteins have been used for  
199 simultaneous protein identification and elemental mapping by correlative fluorescence microscopy  
200 and nanoSIMS [68]. These studies suggest that exogenous elements with a small mass and size are

201 suitable for probing DNA and proteins in the complex cellular environment and can be used in  
202 correlated nanoSIMS studies.

203  
204 **Correlation between more than two subcellular imaging platforms.** The combination of  
205 multiple subcellular imaging platforms can provide a comprehensive view of the ultrastructure,  
206 concentration and distribution of elements (macronutrients and metals) and isotopic ratios, and  
207 molecules from a single region of interest in the cell (Figure 3). This can be performed by analyzing  
208 different consecutive resin sections from the same cell on different platforms [12,13,57]. This  
209 flexible strategy allows one to choose the required thickness and support (e.g. wafer, grid, Si  
210 window) for each section, and detailed ultrastructure can be obtained with EM. Thus, the  
211 morphological and different chemical features can be superimposed. Yet, collecting serial sections  
212 of different thicknesses to target the same cellular region or organelle is a challenge.

213  
214 **Integrated correlative instruments.** A correlative approach can be facilitated when  
215 morphological and chemical information from exactly the same area can be acquired in the same  
216 instrument. One of the best examples is TEM-EDS and EFTEM. The TEM offers the highest  
217 possible resolution for both imaging and element analysis. Provided samples are thin (usually ~150  
218 nm - 200 kV) and the elements of interest can be preserved, simultaneous structural and elemental  
219 information can be obtained at the nanoscale (Figure 3) [69]. However, molecular information is  
220 not available and absolute quantitation can be difficult. Using synchrotron X-rays nanoprobe, the  
221 combination between **X-ray phase contrast tomography** and X-ray fluorescence microscopy can  
222 provide the morphological information and quantification of elements, respectively (Figure 3).  
223 This has been recently performed on a freeze-dried human phagocytic cell [16] and human red  
224 blood cells infected with the malaria parasite *Plasmodium falciparum* [70]. An alternative to phase  
225 contrast imaging is ptychography [71], which can be combined with XRF tomography to obtain  
226 the 3D localization of elements in cells, such as bacteria in [72].

227 New instruments that offer simultaneous morphological and molecular information are emerging  
228 but are yet to be applied to biological specimens. For instance, the HIM-SIMS (Secondary Ion  
229 Mass Spectrometry in the Helium-Ion Microscopy) can combine high-resolution morphological  
230 images with elemental and isotopic maps from SIMS [73]. In contrast to EDS on an SEM, HIM-  
231 SIMS provides better detection limits for elements (including the very light ones) and

232 differentiation between isotopes. However, using HIM-SIMS for stable-isotope labelling  
233 experiments will require a significant improvement of the mass resolution. Overall, the  
234 combination of high-resolution secondary electron images and mass-separated sputtered ion  
235 distributions has high potential to answer open questions in cell biology.

236  
237 **Image processing for multimodal correlative imaging.** Upon acquisition on different imaging  
238 platforms, micrographs need to be processed to correlate or even overlap information from the  
239 same cellular region. Multimodal 2D microscopy requires registration algorithms that can analyze  
240 the same region but at different fields-of-views and resolutions from images acquired with  
241 different excitation probes (e.g. photons, electrons and ions) as well as different detectors.  
242 Compared to monomodal images processing, more sophisticated approaches are needed for  
243 multimodal images since the pixel-intensity of features is not comparable or do not even occur in  
244 both images. The additional challenge in multimodal data sets is the shape of the object that might  
245 be different because of preparation steps or different probing depths of the microscopes.  
246 Distortions may also be introduced when subsequent sections, representing different depth layers  
247 of the sample, are used for correlative imaging. In this context, the ImageJ-based software Correlia  
248 has been recently developed for the registration of 2D-2D multi-modal microscopy data-sets  
249 (available on request).

250

## 251 **Perspectives and future challenges for multimodal subcellular imaging.**

252  
253 **Subcellular mapping metabolites in cells.**

254 Visualization of the compartmentalized distribution of metabolites in cells is one of the most  
255 promising research avenues in biology. Recently, laser-based ionization mass spectrometry  
256 techniques have been successfully used in single-cell metabolomics profiling experiments, but the  
257 lateral resolution precludes imaging subcellular chemistry [74]. Mapping metabolites at  
258 subcellular level can be now envisioned with the revolutionary SIMS instrument Hybrid SIMS  
259 (3D OrbiSIMS, IONTOF) that combines the speed and high lateral resolution imaging capabilities  
260 of ToF-SIMS with unprecedented mass resolution (240K), mass accuracy (sub-ppm), dynamic  
261 range (S/N ratio~ $10^5$ ), and MS/MS capabilities of the Orbitrap Q-Exactive [75]. The instrument  
262 has been used to map the distribution of lipids and neurotransmitters in the hippocampal region

263 of the mouse brain at the cellular and subcellular level. The 3D imaging capabilities were used  
264 to visualizing the accumulation of amiodarone in single lung macrophage cells, and assessing  
265 its toxic effect by correlating drug concentration with the levels of phospholipids and  
266 cholesterol [75].

267  
268 **Future improvements needed to probe cells in their native state and in four dimensions.** The  
269 future of chemical imaging largely relies in the development of cryo-analyses and associated  
270 correlative workflows to allow multiscale chemical analysis of cells in their native state across  
271 multiple instruments. Currently, cryo-analyses present limitations in regard to the suitability of  
272 samples for cryo-preservation and their transfer between different platforms without ice  
273 contamination. In most cases, frozen cells must be sectioned/milled in order to visualize the  
274 interior. Future expansion in this area will require improvements in preparation of quality cryo-  
275 sections (e.g. cryo-FIB-SEM), development of cryo-enabled instrument platforms (e.g.  
276 nanoSIMS), and the capability to transfer samples seamlessly between these. Additional  
277 challenges associated to cryo-imaging are the low contrast of vitrified cells and possible  
278 devitrification under irradiation from the probe (e.g. ions, X-rays).

279 Chemical information in 2D is insufficient to fully describe the compartmentalization of an  
280 element/molecule throughout an entire cell, especially when information comes from a single thin  
281 section (60-300 nm thickness) of a cell. Techniques to acquire 3D structural information at the  
282 subcellular level are readily available (e.g. FIB-SEM) but it is difficult to couple these with  
283 analytical information. Synchrotron-based coherent X-ray scattering techniques such as  
284 holotomography or ptychography have both demonstrated constant improvements toward  
285 ultrastructural 3D characterization of a cell architecture [76]. We therefore foresee a bright future  
286 in the coupling between these techniques with X-ray fluorescence tomography for 3D elemental  
287 imaging.

288 The down side of high-resolution chemical imaging is the low throughput, which precludes for  
289 robust statistical analyses. We can expect that ultra-high-speed scanning strategy and highly  
290 efficient detection will be the next steps to foster on the instrumentation side. For example,  
291 extremely brilliant X-ray synchrotron source and high-rate scanning strategies become reality with  
292 the upgrade of the synchrotrons, such as the European Synchrotron Radiation Facility (ESRF) [77].

293 Finally, future developments need to integrate a biologically-relevant temporal dimension into the  
294 correlative imaging workflow towards 4D imaging. Because probing elements and molecules of  
295 live cells at the nanoscale level remain very challenging, there is a need to capture multiple  
296 snapshots of a phenotypic state of a cell over time to follow and better understand dynamic cellular  
297 processes following exposure to abiotic or biotic stress. One single snapshot may provide a biased  
298 vision of the phenotypic response of a cell if imaging analysis occurs on the inappropriate  
299 timescale. Temporal resolution can be obtained by the coupling with live imaging (fluorescent and  
300 super resolution microscopy) and developing microfluidic devices [78], or rapid cryo-fixation  
301 strategies [79]. For instance, dynamic fluorescent light microscopy can be rapidly followed by  
302 cryo-immobilization in few seconds for CLEM studies thanks to new tools (e.g. CryoCapsule),  
303 and could be extended to chemical imaging in the future [80]. In addition, recent advances in super-  
304 resolution fluorescence microscopy (e.g. Stimulated emission depletion - STED - microscopy)  
305 [81] and future development of new fluorescent element-specific probes will potentially provide a  
306 dynamic view of labile elements (e.g.  $\text{Ca}^{2+}$ ,  $\text{Fe}^{2+/3+}$ ,  $\text{Zn}^{2+}$ ) in live cells at 10-50 nm resolution [82].  
307 Correlation with chemical imaging will open new perspectives for bridging temporal and spatial  
308 resolution [83].  
309 Thus, the development of time-resolved 3D subcellular imaging in cryo-conditions will be a major  
310 breakthrough in cell biology to capture dynamic subcellular processes in a native-state cell.  
311

### **Outstanding Questions**

- Is it possible to preserve the native physiological state of a cell from sample preparation to subcellular imaging? How can structural and chemical preservation of the cell be carefully assessed and artefacts identified to avoid misleading results?
- Can we resolve the chemical landscape (composition and distribution of elements and molecules) of a cell with high spatial resolution, in three dimensions and over a relevant temporal scale? What would be the analytical workflow to implement for 4D subcellular imaging?
- What are the methodological and technological strategies to analyze the same subcellular region of interest across different subcellular imaging techniques?
- How can we include cryo-analysis in the workflow of correlative subcellular imaging, from sample preparation to obtain vitreous cells, to transfer and imaging across different platforms? Can it be applied to different types of cells from a tissue or isolated in culture or the environment?

- How can the throughput of chemical imaging techniques be increased to observe large numbers of biological samples and perform robust statistical comparisons?

- Can we enhance the mass and spatial resolution of SIMS imaging instruments in order to visualize a large number of different metabolites in the cell?

312

### 313 **Concluding Remarks**

314 Subcellular chemical imaging techniques are constantly improving and becoming ever-more  
315 powerful tools for quantitative visualization of elements, isotopes, and molecules in cells.  
316 However, untangling their complex requirements and capabilities is a vital step in ensuring that  
317 researchers can apply such methods to outstanding research questions and problems. With this,  
318 appropriate sample preparation and suitable imaging platform(s) need to be selected according to  
319 the sample, spatial resolution, and targeted elements/molecules. In this review, we have outlined  
320 the principles of key analytical instrumentation, discussed strategies for sample preparation, and  
321 highlighted the potential for correlative electron microscopy and chemical imaging to accumulate  
322 structural and chemical information from a single region of a cell. Correlated morphological and  
323 chemical imaging has the potential to spur a rapid expansion in different fields, such as cell  
324 biology, biomedicine, ecophysiology, pharmacology, toxicology, biogeochemistry. In the near  
325 future, we do not foresee a technique that would encompass all the capabilities to explore the  
326 chemical/molecular/isotopic composition and ultrastructure of a cell. Thus, the development of  
327 integrative studies and dedicated analytical correlative workflows, from sample preparation to  
328 multimodal imaging and image processing, will be a major contribution towards a full  
329 comprehension of the physiology of a cell at the subcellular level.

330

### **Glossary**

- **Chemical imaging:** spatial characterization of the chemical composition of a sample (isotopes, elements, molecules). This can be achieved by multiple high-resolution imaging platforms, using different physical processes to interrogate subcellular information (e.g. X-ray fluorescence, ionization)

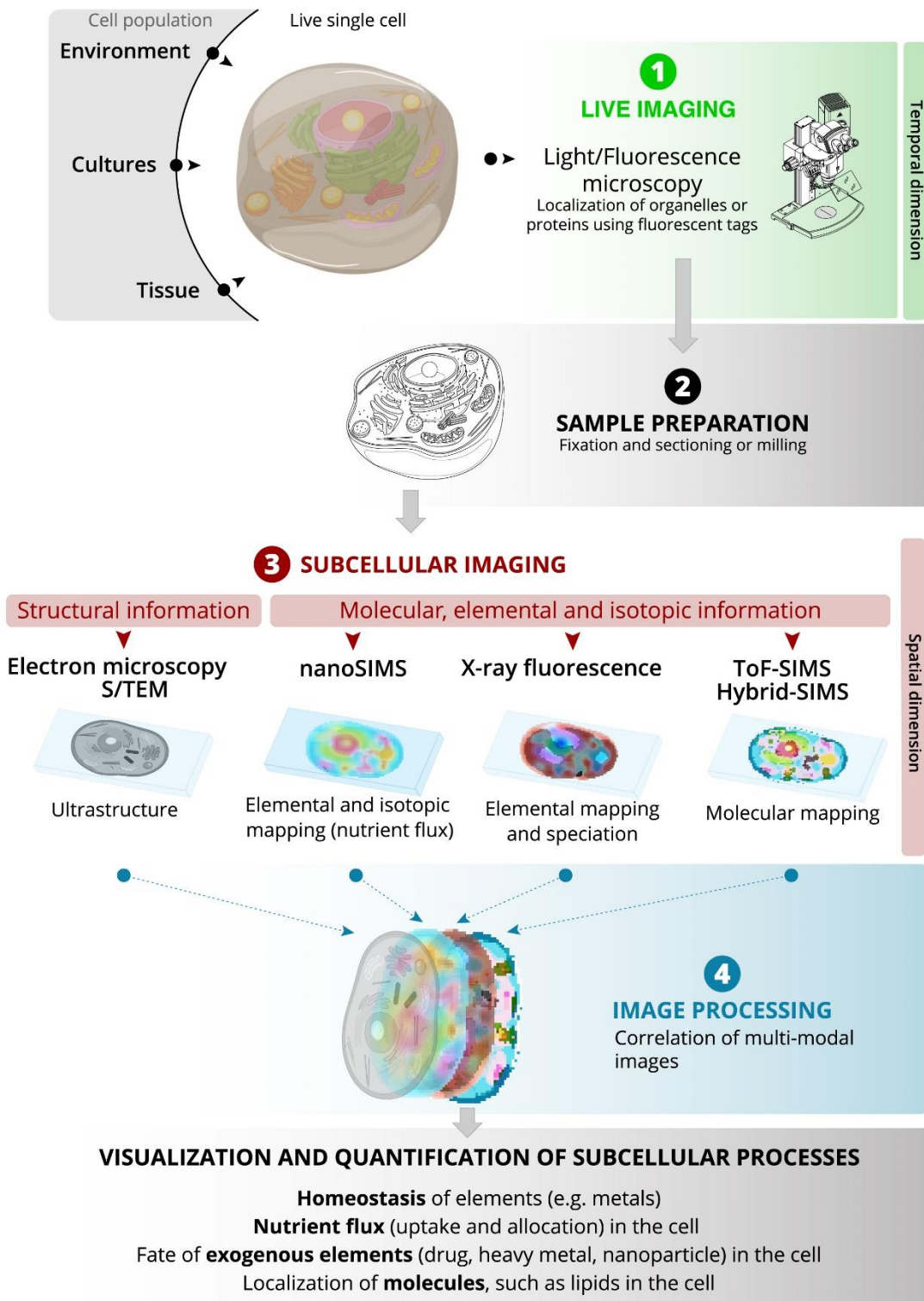
- **Chemical landscape:** Composition and distribution patterns of elements, isotopes and molecules in a sample (e.g. cell). Its visualization cannot be obtained with a single imaging platform but different techniques need to be used in a correlative way.
- **Correlative electron microscopy and chemical imaging:** workflow to prepare samples, obtain micrographs from different complementary imaging platforms, and overlap morphological and chemical (elements/molecules) information from the same region of a specimen.
- **HybridSIMS:** [Bi]<sub>n</sub> (n=1, 3, 5, 7) or [Ar]<sub>n</sub> (n~1000) gas-cluster ion source are used for analysis of large molecular ions. The OrbiTrap analyzer provide a MRP of ~10E5 that enables a precise compound identification.
- **Multimodal imaging:** Microscopy observations of the same sample using more than two imaging platforms to obtain complementary morphological and chemical information (e.g. light and electron microscopy, nanoSIMS and S-XRF).
- **nanoSIMS:** single-atomic Cs<sup>+</sup> or O<sup>-</sup> primary ions are used for both sputtering and analysis, the ionized material is then analyzed by a Mattauch-Herzog mass spectrometer that allows for the parallel detection of max 7 masses. The high energy of the primary ions causes a strong fragmentation of molecules down to single-atomic ions allowing for quantitation of changes in isotopic composition.
- **SIMS:** secondary ion mass spectrometry whereby secondary ions are sputtered away from the topmost layer of a sample by a focused primary ion beam and analyzed in a mass spectrometer. NanoSIMS, ToF-SIMS and HybridSIMS are SIMS imaging techniques with primary ion beams of different sources and energies, and with different mass spectrometers to probe elements, isotopes and small molecules.
- **ToF-SIMS:** pulsed [Bi]<sub>n</sub> (n=1, 3, 5, 7) or [Ar]<sub>n</sub> (n~1000) cluster ion sources are mainly used for analysis while Ar [n] cluster, Cs<sup>+</sup> or O<sup>-</sup> can be used as sputtering sources. The use of cluster ions for analysis reduces the fragmentation upon impact, leading to the preservation of molecular species. The Time-of-Flight mass spectrometer allows the simultaneous detection of all masses.
- **Vitreous cell:** Frozen hydrated cell with amorphous ice (i.e. without crystals that can alter the ultrastructure and chemical composition of cells). Vitreous cell can be obtained using high-pressure freezing or plunge freezing machines.

- **X-ray fluorescence microscopy (XRF)**: physical process consisting on the emission of X-rays from a specimen following the excitation of core electrons of atoms; the analysis of the emitted X-rays allows the identification of the elemental content of the specimen. The excitation of electrons can be achieved by a beam of electrons, protons or photons.

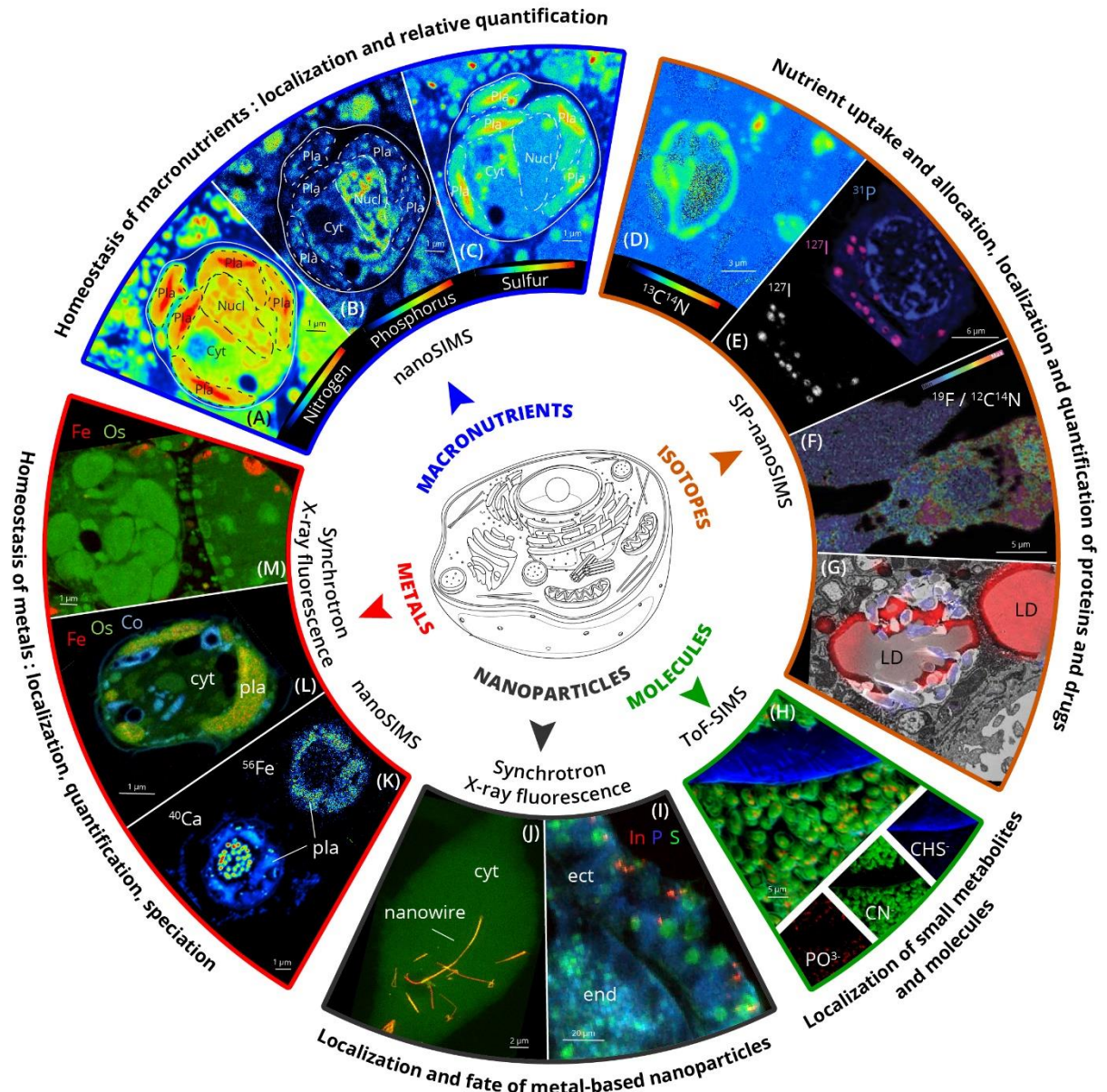
- **X-ray phase contrast tomography**: Tomographic technique sensitive to refraction of X-rays in matter, leading to phase variations of the X-rays depending on the sample's electron density, and particularly adapted to reveal weakly absorbing features like those present in biological samples.

331

332



335 **Figure 1 - Key figure. Outline of correlative multimodal subcellular imaging workflow**  
336 **including electron and chemical imaging.** Individual cells can be isolated from a population in  
337 a tissue, culture or in the environment, and observed *in vivo* using light/fluorescence microscopy  
338 for dynamic and functional imaging. After sample preparation (fixation and sectioning/milling), a  
339 cell can be analyzed by different high-resolution imaging platforms in a correlative way. Electron  
340 microscopy can unveil detailed ultrastructure of the cell while chemical imaging platforms  
341 (nanoSIMS, X-ray fluorescence, ToF-SIMS, Hybrid-SIMS) enable the visualization and  
342 quantification of elements, isotopes and molecules at the subcellular level. Finally, image  
343 processing allows the correlation between multimodal micrographs that contain complementary  
344 information of the cell. This workflow still requires some methodological developments at  
345 different steps, from sample preparation to image processing, in order to further understand the  
346 metabolism and physiology of a cell at the nanoscale in its close-to-native state.



347  
 348 **Figure 2.** The potential of chemical imaging to unveil the chemical landscape of a cell:  
 349 **composition and distribution of elements, isotopes and molecules at the nanoscale.**  
 350 (A-B-C) NanoSIMS images showing the distribution of the macronutrients nitrogen (A;  $^{12}\text{C}^{14}\text{N}^-$ ),  
 351 phosphorous (B;  $^{31}\text{P}^-$ ), and sulfur (C;  $^{32}\text{S}^-$ ) inside a microalgal cell.  
 352 (D) NanoSIMS image showing the uptake of  $^{13}\text{C}$  incorporated in proteins ( $^{13}\text{C}^{14}\text{N}^-$ ) in cells after  
 353 incubation in  $^{13}\text{C}$ -labelled bicarbonate (SIP-nanoSIMS).  
 354 (E) NanoSIMS image acquired on macrophages treated with the drug Iodine-containing  
 355 amiodarone. The overlay of  $^{31}\text{P}^-$  (blue) and  $^{127}\text{I}^-$  (purple) secondary ions map provides

356 morphological information (localization of the nucleus) and shows specific localization of the drug  
357 within the lysosomes. Reproduced with permission from [84].

358 **(F)** Specific labeling of proteins for correlated fluorescence microscopy and nanoSIMS using  
359 FluorLink–nanobody anti-GFP and direct immunostaining strategies. NanoSIMS image of  
360  $^{19}\text{F}/^{12}\text{C}^{14}\text{N}$  ratio shows the presence of the targeted protein in specific cellular areas. Reproduced  
361 with permission from [65].

362 **(G)** Visualization of antibiotic in cells. Overlay of nanoSIMS and electron microscopy images  
363 showing the accumulation of the antibiotic in lipid droplets (LD). The bromine-containing  
364 antibiotic (bedaquiline) can be detected and semi-quantified by the nanoSIMS through the  $^{79}\text{Br}$   
365 ions (red signal). Reproduced with permission from [41].

366 **(H)** ToF-SIMS images showing accumulation of phosphates (red,  $\text{PO}_3^-$ ) in biofilm of algal cells  
367 (green,  $\text{CN}^-$ ) growing in cotton (blue,  $\text{CH}_4\text{S}^-$ ). Reproduced with permission from [47].

368 **(I)** Synchrotron X-ray Fluorescence image showing the distribution of indium phosphide-based  
369 nanocrystals in a frozen section of the *Hydra vulgaris*. Nanocrystals (detected by indium X-ray  
370 fluorescence, in red) are mainly internalized in the ectoderm layer (ect). The natural macronutrients  
371 phosphorous (blue) and sulfur (green) provide the morphological context. Reproduced with  
372 permission from [21].

373 **(J)** Synchrotron X-ray Fluorescence image showing the presence of silver nanowires in a fibroblast  
374 cell (S in green, and Ag in red). Yellow regions indicate colocalization of Ag and S inside the cell.  
375 Reproduced with permission from [4]. Copyright 2019 National Academy of Sciences.

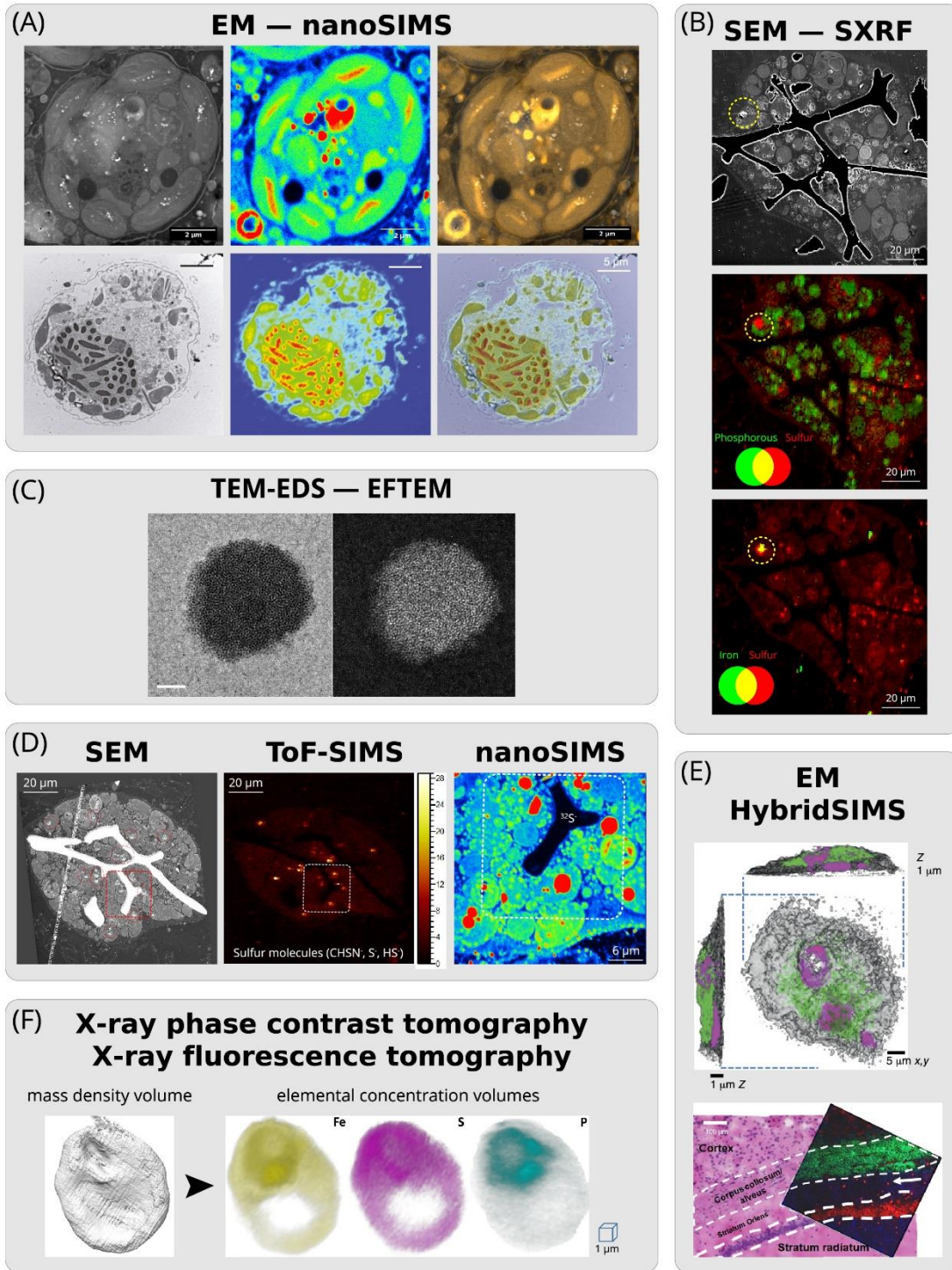
376 **(K)** NanoSIMS image showing the distribution of Ca ( $^{40}\text{Ca}^+$ ) and Fe ( $^{56}\text{Fe}^+$ ) in a microalga.  
377 Calcium mapping unveils the overall morphology of the cells with high concentration in the  
378 nucleus (nucl). Iron is mostly contained in the plastids (pla).

379 **(L-M)** Synchrotron X-Ray Fluorescence images showing the subcellular distribution and  
380 quantification of the trace metals Fe (red) and Co (blue), and Os (green) in microalgal cells.

381 Abbreviations: Pla: plastid of microalgal cell; Cyt: cytoplasm; Nucl: nucleus; LD: Lipid droplet;  
382 ect: ectoderm; end: endoderm.

383

384



385

386 **Figure 3.** Examples of correlated electron microscopy and chemical imaging.

387 (A) Correlation between electron microscopy (left images) and nanoSIMS (middle images)  
388 showing the sulfur ( $^{32}\text{S}^-$ , upper image) and nitrogen ( $^{12}\text{C}^{14}\text{N}^-$ , lower image) content in a microalgal  
389 cell. Right images show the overlay of macronutrient mapping and ultrastructure obtained from  
390 consecutive sections or the same section. Image courtesy of Charlotte Lekieffre.

391 (B) Correlation between scanning electron microscopy (SEM) and Synchrotron X-Ray  
392 Fluorescence microscopy (S-XRF). SEM observation has been performed on the same cell section  
393 after S-XRF analysis. S-XRF mapping of phosphorous and iron (green), and sulfur (red) unveils  
394 numerous hotspots (one example highlighted by the yellow circle) where sulfur and iron are  
395 colocalized in high concentration in the cell.

396 (C) TEM image (left) with corresponding EFTEM (Energy-Filtered Transmission Electron  
397 Microscopy Fe map (right) showing aggregated ferritin molecules within a cell (courtesy Jeremy  
398 Shaw and David Keays). Scale bar = 100 nm.

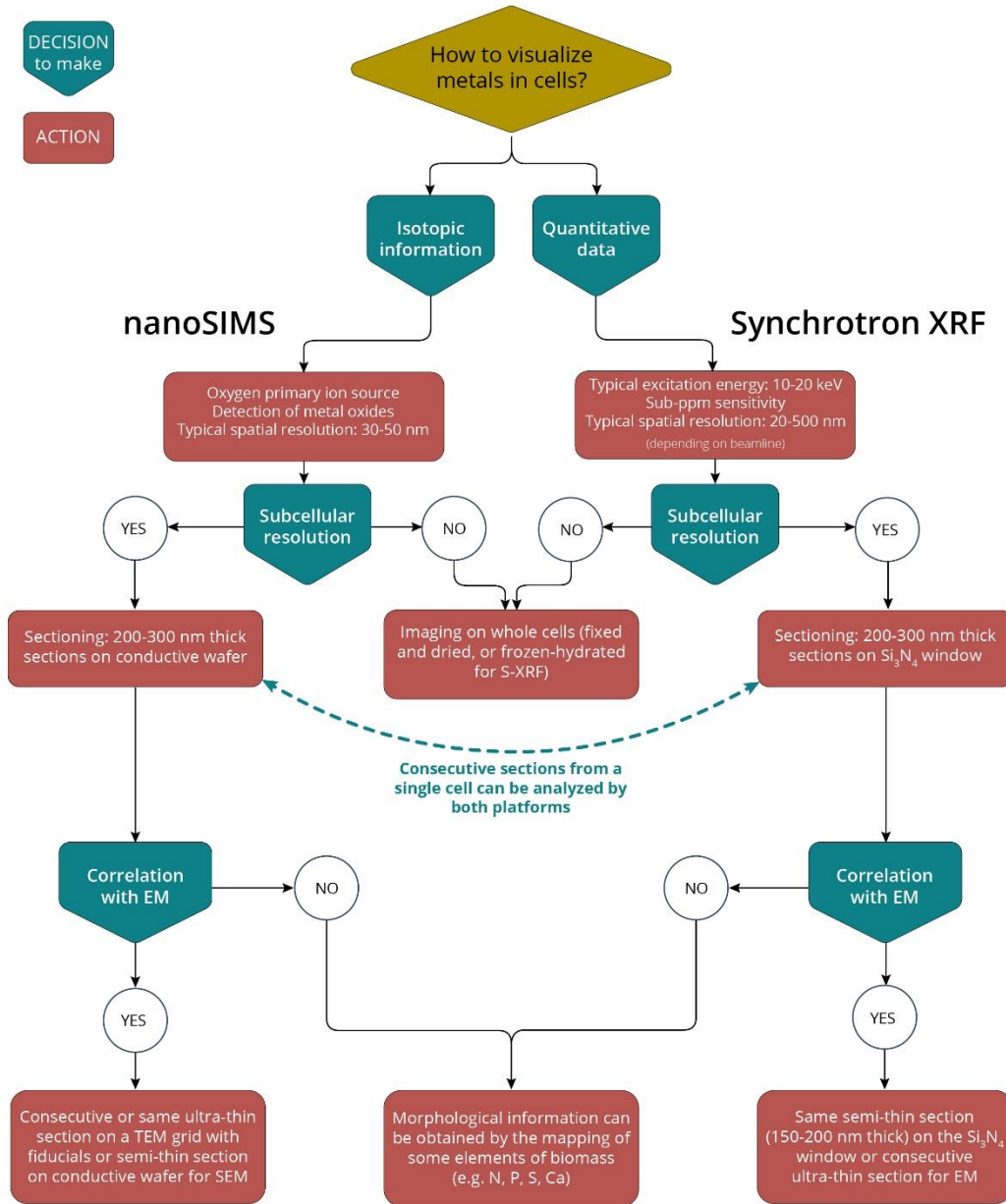
399 (D) Correlation between Scanning Electron Microscopy, ToF-SIMS and nanoSIMS showing the  
400 cell ultrastructure, distribution of sulfur molecules ( $\text{CHSN}^-$ ,  $\text{S}^-$ ,  $\text{HS}^-$ ) and sulfur ( $^{32}\text{S}^-$ ), respectively.  
401 These multimodal images were acquired from consecutive thin sections.

402 (E) EM- Hybrid SIMS image showing the 3D distribution in a single cell of the drug amiodarone  
403 ( $m/z$  646, green) and biomolecules at  $m/z$  157 (purple) and  $m/z$  184 (green) (upper image). Lower  
404 image obtained from the hybrid SIMS instrument shows that C24:1 sulfatides ( $m/z$  888.62, green)  
405 are localized to the *corpus collosum*. DNA base adenine (red,  $m/z$  134.05), a nuclear marker, shows  
406 that neurons are densely packed in the pyramidal layer and sparsely packed in the Stratum Oriens,  
407 where phosphoinositol is located ( $m/z$  241.01, blue). Figure adapted with permission from [75].

408 (F) Direct correlation between X-ray phase contrast and X-ray fluorescence tomography on a  
409 malaria-infected cell. The 3D mass density volume is obtained as after tomographic reconstruction  
410 (on the left). Subsequent X-ray fluorescence scanning measurements were performed on the same  
411 sample showing the 3D mass concentration volumes of iron, sulfur, and phosphorous (on the right).  
412 Reproduced with permission from [70].

413

414



415

416 **Figure 4. How to visualize metals in cells?**

417 Decision flowchart to guide users for probing metals in a single cell at high resolution and  
418 sensitivity..

## 419 **Acknowledgements**

420 J.D was supported by the LabEx GRAL (ANR-10-LABX-49-01), Pôle CBS from the University  
421 of Grenoble Alpes, and Défi X-Life grant from CNRS. The authors acknowledge the support and  
422 use of resources from Instruct (a Landmark ESFRI project) and the ESRF for providing beamtime.  
423 We are thankful for the use of the analytical facilities of the Centre for Chemical Microscopy  
424 (ProVIS) at UFZ Leipzig, which is supported by European Regional Development Funds (EFRE—  
425 Europe funds Saxony) and the Helmholtz Association. This research is also supported by EMBRC-  
426 France, whose French state funds are managed by the ANR within the Investments of the Future  
427 program under reference ANR-10-INBS-02. We also thank Yannick Schwab for critically reading  
428 the manuscript and suggesting improvements. We are grateful to colleagues for sharing  
429 microscopy images.

430

## 431 **References**

- 432 1 Salt, D.E. *et al.* (2008) Ionomics and the study of the plant ionome. *Annual review of plant biology*  
433 59, 709–733
- 434 2 Hackett, M.J. *et al.* (2019) Elemental characterisation of the pyramidal neuron layer within the rat  
435 and mouse hippocampus. *Metallomics* 11, 151–165
- 436 3 Veronesi, G. *et al.* (2016) Visualization, quantification and coordination of Ag<sup>+</sup> ions released  
437 from silver nanoparticles in hepatocytes. *Nanoscale* 8, 17012–17021
- 438 4 Lehmann, S.G. *et al.* (2019) Crumpling of silver nanowires by endolysosomes strongly reduces  
439 toxicity. *Proceedings of the National Academy of Sciences* 116, 14893–14898
- 440 5 de Boer, P. *et al.* (2015) Correlated light and electron microscopy: ultrastructure lights up! *Nature*  
441 *Methods* 12, 503–513
- 442 6 Karreman, M.A. *et al.* (2016) Intravital Correlative Microscopy: Imaging Life at the Nanoscale.  
443 *Trends in Cell Biology* 26, 848–863
- 444 7 da Cunha, M.M.L. *et al.* (2016) Overview of chemical imaging methods to address biological  
445 questions. *Micron* 84, 23–36
- 446 8 Baker, T.C. *et al.* (2017) Recent advancements in matrix-assisted laser desorption/ionization mass  
447 spectrometry imaging. *Current Opinion in Biotechnology* 43, 62–69
- 448 9 Lauwers, M. *et al.* (2013) An iron-rich organelle in the cuticular plate of avian hair cells. *Current*  
449 *Biology* 23, 924–929
- 450 10 Cotte, M. *et al.* (2017) The ID21 X-ray and infrared microscopy beamline at the ESRF: status and  
451 recent applications to artistic materials. *J. Anal. At. Spectrom.* 32, 477–493

- 452 11 Pushie, M.J. *et al.* Elemental and chemically specific x-ray fluorescence imaging of biological  
453 systems. , *Chemical Reviews*, 114. (2014) , 8499–8541
- 454 12 Decelle, J. *et al.* (2019) Algal Remodeling in a Ubiquitous Planktonic Photosymbiosis. *Current*  
455 *Biology* DOI: 10.1016/j.cub.2019.01.073
- 456 13 Kashiv, Y. *et al.* (2016) Imaging trace element distributions in single organelles and subcellular  
457 features. *Scientific Reports* 6, 21437
- 458 14 Adams, M.S. *et al.* (2016) Copper Uptake, Intracellular Localization, and Speciation in Marine  
459 Microalgae Measured by Synchrotron Radiation X - ray Fluorescence and Absorption  
460 Microspectroscopy. DOI: 10.1021/acs.est.6b00861
- 461 15 Ciccotosto, G.D. *et al.* (2014) Quantitation and localization of intracellular redox active metals by  
462 X-ray fluorescence microscopy in cortical neurons derived from APP and APLP2 knockout tissue.  
463 *Metallomics* 6, 1894–1904
- 464 16 Gramaccioni, C. *et al.* (2018) Nanoscale quantification of intracellular element concentration by  
465 X-ray fluorescence microscopy combined with X-ray phase contrast nanotomography. *Applied*  
466 *Physics Letters* 112,
- 467 17 Brown, K. *et al.* (2018) Intracellular in situ labeling of TiO<sub>2</sub> nanoparticles for fluorescence  
468 microscopy detection. *Nano Research* 11, 464–476
- 469 18 Fus, F. *et al.* (2019) Intracellular Localization of an Osmocenyl-Tamoxifen Derivative in Breast  
470 Cancer Cells Revealed by Synchrotron Radiation X-ray Fluorescence Nanoimaging. *Angewandte*  
471 *Chemie International Edition* 58, 3461–3465
- 472 19 Kapishnikov, S. *et al.* (2019) Mode of action of quinoline antimalarial drugs in red blood cells  
473 infected by Plasmodium falciparum revealed in vivo. *Proceedings of the National Academy of*  
474 *Sciences* DOI: 10.1073/pnas.1910123116
- 475 20 Sanchez-Cano, C. *et al.* (2019) Nanofocused synchrotron X-ray absorption studies of the  
476 intracellular redox state of an organometallic complex in cancer cells. *Chemical Communications*  
477 55, 7065–7068
- 478 21 Veronesi, G. *et al.* (2019) In Vivo Biotransformations of Indium Phosphide Quantum Dots  
479 Revealed by X-Ray Microspectroscopy. *ACS Applied Materials & Interfaces* 11, 35630–35640
- 480 22 Hackett, M.J. *et al.* (2016) Chemical biology in the embryo: In situ imaging of sulfur biochemistry  
481 in normal and proteoglycan-deficient cartilage matrix. *Biochemistry* 55, 2441–2451
- 482 23 Gyngard, F. and Steinhäuser, M.L. (2019) Biological explorations with nanoscale secondary ion  
483 mass spectrometry. *Journal of Analytical Atomic Spectrometry* 34, 1534–1545
- 484 24 Agüi-Gonzalez, P. *et al.* (2019) SIMS imaging in neurobiology and cell biology. *Journal of*  
485 *Analytical Atomic Spectrometry* 34, 1355–1368
- 486 25 Malherbe, J. *et al.* (2016) A new RF plasma oxygen primary ion source on NanoSIMS for  
487 improved lateral resolution and detection of electropositive elements at single cell level. *Analytical*  
488 *Chemistry* DOI: 10.1021/acs.analchem.6b01153
- 489 26 Nuñez, J. *et al.* (2018) NanoSIMS for biological applications: Current practices and analyses.  
490 *Biointerphases* 13, 03B301

- 491 27 Weng, N. *et al.* (2017) In situ subcellular imaging of copper and zinc in contaminated oysters  
 492 revealed by nanoscale secondary ion mass spectrometry. *Environmental Science & Technology*  
 493 DOI: 10.1021/acs.est.7b05090
- 494 28 Tsednee, M. *et al.* (2019) Manganese co-localizes with calcium and phosphorus in  
 495 *Chlamydomonas acidocalcisomes* and is mobilized in Mn-deficient conditions. *Journal of*  
 496 *Biological Chemistry* DOI: 10.1074/jbc.RA119.009130
- 497 29 Mayali, X. (2020) NanoSIMS: Microscale Quantification of Biogeochemical Activity with Large-  
 498 Scale Impacts. *Annual Review of Marine Science* 12, 1–19
- 499 30 Musat, N. *et al.* (2016) Tracking microbial interactions with NanoSIMS. *Current Opinion in*  
 500 *Biotechnology* 41, 114–121
- 501 31 Stryhanyuk, H. *et al.* (2018) Calculation of single cell assimilation rates from sip-nanosims-  
 502 derived isotope ratios: A comprehensive approach. *Frontiers in Microbiology* 9, 1–15
- 503 32 Berthelot, H. *et al.* (2018) NanoSIMS single cell analyses reveal the contrasting nitrogen sources  
 504 for small phytoplankton. *The ISME Journal* DOI: 10.1038/s41396-018-0285-8
- 505 33 Terrado, R. *et al.* (2017) Autotrophic and heterotrophic acquisition of carbon and nitrogen by a  
 506 mixotrophic chrysophyte established through stable isotope analysis. *ISME Journal* 11, 2022–  
 507 2034
- 508 34 He, C. *et al.* (2018) NanoSIMS imaging reveals unexpected heterogeneity in nutrient uptake by  
 509 brown adipocytes. *Biochemical and Biophysical Research Communications* 504, 899–902
- 510 35 Lekieffre, C. *et al.* (2018) Inorganic carbon and nitrogen assimilation in cellular compartments of  
 511 a benthic kleptoplastic foraminifer. *Scientific Reports* 8, 1–12
- 512 36 Volland, J.M. *et al.* (2018) NanoSIMS and tissue autoradiography reveal symbiont carbon fixation  
 513 and organic carbon transfer to giant ciliate host. *ISME Journal* 12, 714–727
- 514 37 Gibbin, E. *et al.* (2019) *Vibrio coralliilyticus* infection triggers a behavioural response and  
 515 perturbs nutritional exchange and tissue integrity in a symbiotic coral. *ISME Journal* 13, 989–1003
- 516 38 Martínez-Pérez, C. *et al.* (2016) The small unicellular diazotrophic symbiont, UCYN-A, is a key  
 517 player in the marine nitrogen cycle. *Nature Microbiology* 1, 16163
- 518 39 Pasulka, A.L. *et al.* (2018) Interrogating marine virus-host interactions and elemental transfer with  
 519 BONCAT and nanoSIMS-based methods. *Environmental Microbiology* 20, 671–692
- 520 40 Worrlich, A. *et al.* (2017) Mycelium-mediated transfer of water and nutrients stimulates bacterial  
 521 activity in dry and oligotrophic environments. *Nature Communications* 8,
- 522 41 Greenwood, D.J. *et al.* (2019) Subcellular antibiotic visualization reveals a dynamic drug reservoir  
 523 in infected macrophages. *Science (New York, N.Y.)* 364, 1279–1282
- 524 42 Vanbellinghen, Q.P. *et al.* (2015) Time-of-flight secondary ion mass spectrometry imaging of  
 525 biological samples with delayed extraction for high mass and high spatial resolutions. *Rapid*  
 526 *Communications in Mass Spectrometry* 29, 1187–1195
- 527 43 Benettoni, P. *et al.* (2019) Identification of nanoparticles and their localization in algal biofilm by  
 528 3D-imaging secondary ion mass spectrometry. *Journal of Analytical Atomic Spectrometry* DOI:

- 529 10.1039/C8JA00439K
- 530 44 Henss, A. *et al.* (2018) High resolution imaging and 3D analysis of Ag nanoparticles in cells with  
531 ToF-SIMS and delayed extraction. *Biointerphases* 13, 03B410
- 532 45 Raina, J.-B. *et al.* (2017) Subcellular tracking reveals the location of dimethylsulfoniopropionate  
533 in microalgae and visualises its uptake by marine bacteria. *eLife* 6, 1–17
- 534 46 Dowlatshahi Pour, M. *et al.* (2019) Mass spectrometry imaging as a novel approach to measure  
535 hippocampal zinc. *Journal of Analytical Atomic Spectrometry* 34, 1581–1587
- 536 47 Osorio, J.H.M. *et al.* (2019) Investigation of architecture development and phosphate distribution  
537 in *Chlorella* biofilm by complementary microscopy techniques. *FEMS Microbiology Ecology* 95,  
538 1–10
- 539 48 Sämfors, S. *et al.* (2019) Localised lipid accumulation detected in infarcted mouse heart tissue  
540 using ToF-SIMS. *International Journal of Mass Spectrometry* 437, 77–86
- 541 49 Passarelli, M.K. *et al.* (2013) Single-cell lipidomics: Characterizing and imaging lipids on the  
542 surface of individual *Aplysia californica* neurons with cluster secondary ion mass spectrometry.  
543 *Analytical Chemistry* 85, 2231–2238
- 544 50 Moore, K.L. *et al.* (2014) Combined NanoSIMS and synchrotron X-ray fluorescence reveal  
545 distinct cellular and subcellular distribution patterns of trace elements in rice tissues. *New*  
546 *Phytologist* 201, 104–115
- 547 51 Zhou, J. *et al.* (2011) Reproducibility and quantitation of amplicon sequencing-based detection.  
548 *The ISME Journal* 5, 1303–1313
- 549 52 Perrin, L. *et al.* (2015) Evaluation of sample preparation methods for single cell quantitative  
550 elemental imaging using proton or synchrotron radiation focused beams. *J. Anal. At. Spectrom.*  
551 DOI: 10.1039/C5JA00303B
- 552 53 Das, S. *et al.* (2019) Manganese Mapping Using a Fluorescent Mn 2+ Sensor and  
553 Nanosynchrotron X-ray Fluorescence Reveals the Role of the Golgi Apparatus as a Manganese  
554 Storage Site. *Inorganic Chemistry* 58, 13724–13732
- 555 54 Carmona, A. *et al.* (2019) Mapping Chemical Elements and Iron Oxidation States in the Substantia  
556 Nigra of 6-Hydroxydopamine Lesioned Rats Using Correlative Immunohistochemistry With  
557 Proton and Synchrotron Micro-Analysis. *Frontiers in Neuroscience* 13, 1–12
- 558 55 Carmona, A. *et al.* (2014) Environmental manganese compounds accumulate as Mn(ii) within the  
559 Golgi apparatus of dopamine cells: relationship between speciation, subcellular distribution, and  
560 cytotoxicity. *Metallomics* 6, 822
- 561 56 Domart, F. *et al.* (2019) Correlating STED and synchrotron XRF nano-imaging unveils the co-  
562 segregation of metals and cytoskeleton proteins in dendrites. *Bioarchive* DOI:  
563 <http://dx.doi.org/10.1101/810754>
- 564 57 Sanchez-Cano, C. *et al.* (2017) Synchrotron X-Ray Fluorescence Nanoprobe Reveals Target Sites  
565 for Organo-Osmium Complex in Human Ovarian Cancer Cells. *Chemistry - A European Journal*  
566 23, 2512–2516
- 567 58 Clode, P.L. *et al.* (2009) In Situ Mapping of Nutrient Uptake in the Rhizosphere Using Nanoscale

- 568 Secondary Ion Mass Spectrometry. *Plant Physiology* 151, 1751–1757
- 569 59 Kopp, C. *et al.* (2015) Subcellular Investigation of Photosynthesis-Driven Carbon Assimilation in  
570 the Symbiotic Reef Coral *Pocillopora damicornis*. *mBio* 6, 1–9
- 571 60 Hu, X. *et al.* (2019) Release of cholesterol-rich particles from the macrophage plasma membrane  
572 during movement of filopodia and lamellipodia. *eLife* 8, 1–26
- 573 61 Musat, N. *et al.* (2012) Detecting metabolic activities in single cells, with emphasis on nanoSIMS.  
574 *FEMS microbiology reviews* 36, 486–511
- 575 62 Saka, S.K. *et al.* (2014) Correlated optical and isotopic nanoscopy. *Nature communications* 5,  
576 3664
- 577 63 Lau, K.H. *et al.* (2010) Development of a new bimodal imaging methodology: a combination of  
578 fluorescence microscopy and high-resolution secondary ion mass spectrometry. *Journal of*  
579 *microscopy* 240, 21–31
- 580 64 Vreja, I.C. *et al.* (2015) Secondary-ion mass spectrometry of genetically encoded targets.  
581 *Angewandte Chemie - International Edition* 54, 5784–5788
- 582 65 Kabatas, S. *et al.* (2019) Fluorinated nanobodies for targeted molecular imaging of biological  
583 samples using nanoscale secondary ion mass spectrometry. *Journal of Analytical Atomic*  
584 *Spectrometry* 34, 1083–1087
- 585 66 Thiery-Lavenant, G. *et al.* (2014) Detection of immunolabels with multi-isotope imaging mass  
586 spectrometry. *Surface and Interface Analysis* 46, 147–149
- 587 67 Angelo, M. *et al.* (2014) Multiplexed ion beam imaging of human breast tumors. *Nature Medicine*  
588 20, 436–442
- 589 68 Kabatas, S. *et al.* (2019) Boron-Containing Probes for Non-optical High-Resolution Imaging of  
590 Biological Samples. *Angewandte Chemie International Edition* 58, 3438–3443
- 591 69 Ismagulova, T. *et al.* (2018) A new simple method for quantification and locating P and N reserves  
592 in microalgal cells based on energy-filtered transmission electron microscopy (EFTEM) elemental  
593 maps. *PLoS ONE* 13, 1–21
- 594 70 Yang, Y. *et al.* (2019) Three-Dimensional Correlative Imaging of a Malaria-Infected Cell with a  
595 Hard X-ray Nanoprobe. *Analytical Chemistry* DOI: 10.1021/acs.analchem.8b05957
- 596 71 Dierolf, M. *et al.* (2010) Ptychographic X-ray computed tomography at the nanoscale. *Nature* 467,  
597 436–439
- 598 72 Victor, T.W. *et al.* (2018) X-ray Fluorescence Nanotomography of Single Bacteria with a Sub-15  
599 nm Beam. *Scientific Reports* 8, 1–8
- 600 73 Wirtz, T. *et al.* (2019) Imaging and Analytics on the Helium Ion Microscope. *Annual Review of*  
601 *Analytical Chemistry* 12, 523–543
- 602 74 Baumeister, T.U.H. *et al.* (2019) Live single-cell metabolomics with matrix-free laser/desorption  
603 ionization mass spectrometry to address microalgal physiology. *Frontiers in Plant Science* 10, 1–9
- 604 75 Passarelli, M.K. *et al.* (2017) The 3D OrbiSIMS—label-free metabolic imaging with subcellular

605 lateral resolution and high mass-resolving power. *Nature Methods* DOI: 10.1038/nmeth.4504

606 76 Deng, J. *et al.* (2018) Correlative 3D x-ray fluorescence and ptychographic tomography of frozen-  
607 hydrated green algae. *Science Advances* 4, 1–11

608 77 Deng, J. *et al.* (2019) The Velociprobe: An ultrafast hard X-ray nanoprobe for high-resolution  
609 ptychographic imaging. *Review of Scientific Instruments* 90, 083701

610 78 Gibbin, E. *et al.* (2018) Using NanoSIMS coupled with microfluidics to visualize the early stages  
611 of coral infection by *Vibrio coralliilyticus*. *BMC Microbiology* 18, 39

612 79 Kontziampasis, D. *et al.* (2019) A cryo-EM grid preparation device for time-resolved structural  
613 studies. *IUCrJ* 6, 1024–1031

614 80 Heiligenstein, X. *et al.* (2014) The CryoCapsule: Simplifying Correlative Light to Electron  
615 Microscopy. *Traffic* 15, 700–716

616 81 Sigal, Y.M. *et al.* (2018) Visualizing and discovering cellular structures with super-resolution  
617 microscopy. *Science* 361, 880–887

618 82 Ackerman, C.M. *et al.* (2017) Analytical Methods for Imaging Metals in Biology: From Transition  
619 Metal Metabolism to Transition Metal Signaling. *Analytical Chemistry* 89, 22–41

620 83 Bernhardt, M. *et al.* (2018) Correlative microscopy approach for biology using X-ray holography,  
621 X-ray scanning diffraction and STED microscopy. *Nature Communications* 9, 1–9

622 84 Jiang, H. *et al.* (2017) High-resolution sub-cellular imaging by correlative NanoSIMS and electron  
623 microscopy of amiodarone internalisation by lung macrophages as evidence for drug-induced  
624 phospholipidosis. *Chemical Communications* 53, 1506–1509

625